# Impact of Inverse Squeezing Flow on the Self-Assembly of Oppositely Charged Colloidal Particles under Electric Field

Jiaxing Yuan,[1,*] Kyohei Takae,[2,†] and Hajime Tanaka[1,2,‡]
[1]*Research Center for Advanced Science and Technology, University of Tokyo, 4-6-1 Komaba, Meguro-ku, Tokyo 153-8904, Japan*
[2]*Department of Fundamental Engineering, Institute of Industrial Science, University of Tokyo, 4-6-1 Komaba, Meguro-ku, Tokyo 153-8505, Japan*

(Received 7 September 2022; accepted 15 November 2022; published 9 December 2022)

Hydrodynamic interactions (HIs) play a critical role in the self-organization of colloidal suspensions and biological solutions. However, their roles have remained elusive particularly for charged soft matter systems. Here we consider the role of HIs in the self-assembly of oppositely charged colloidal particles, which is a promising candidate for electrical tunable soft materials. We employ the fluid particle dynamics method to consider many-body HIs and the coupling between the colloid, ion, and fluid motions. We find that, under a constant electric field, oppositely charged colloidal particles form clusters and percolate into a gel network, unlike bundlelike aggregates aligned in the field direction observed by Brownian dynamics simulations neglecting HIs. We reveal that the cluster-forming tendency originates from the incompressibility-induced "inverse squeezing flow" effect that dramatically slows down the disaggregation of attached colloids. Our findings indicate that the HI selects a unique kinetic pathway to the nonequilibrium colloidal self-assembly.

DOI: 10.1103/PhysRevLett.129.248001

Colloidal self-assembly is a promising bottom-up strategy to create higher-order structures from the elementary building blocks [1–9]. Of particular interest is the electrostatically driven self-assembly in a binary suspension consisting of oppositely charged colloidal particles [7]. By tuning the valence and size ratio, a diverse range of superlattice structures have been observed in experiments [7,10,11] and simulations [12,13]. Besides the equilibrium superlattices formed after waiting for a long time, ranging from hours to days [14], various nonequilibrium self-assembled configurations have also been reported, including NaCl-type cubic aggregates [15], linear chains [15–17], ionic clusters [15,18,19], and gels [13,20–22]. Moreover, unlike their neutral counterparts, charged colloidal particles can be driven by an external electric field, providing an electrically responsive function to the materials [10]. It was uncovered experimentally that a strong electric field can melt the superlattices and form lanes and jammed bands [10,23], applicable to photonics [24]. Simulations of binary charged colloids further reported a detailed phase diagram as a function of the volume fraction and electrostatic coupling, including lane chains at small volume fraction and low screening, lanes with two-dimensional crystalline order perpendicular to the field at high volume fraction, and a lateral network structure between them [25].

A significant effect on the nonequilibrium self-assembly of charged colloidal systems may arise from hydrodynamic interactions (HIs), which dynamically couple the motion of many colloids and deform ionic clouds. Because of the technical difficulty and computational cost of including HIs in electrokinetic simulations [26–30], most simulations of binary charged colloids have employed the Brownian dynamics (BD) method with a screened Yukawa potential that neglects both HI and ion cloud deformation [15,19,20,22,23,25]. However, the phase ordering kinetics and nonequilibrium electromigration are significantly influenced by HIs [31], with examples including colloidal phase separation and gelation [32–36], polymer collapsing [37], and protein folding [38,39]. The assumption of the fixed screened electrostatics and the neglect of HIs might be allowed at a moderate to high salt concentration and colloidal volume fraction. For example, earlier simulations showed that the inclusion of HIs in the Rotne-Prager form has negligible impact on the lane formation [40], and the BD simulations reproduced the experiments [23]. Nevertheless, this assumption is hardly valid in the opposite limit, e.g., dilute colloidal suspensions with low salinity, which are relevant in many colloidal experiments [41–43]. Thus, there is a pressing need to explore this strong coupling regime where proper incorporations of both long-range electrostatic interactions and HIs are essential.

In this Letter, we use the fluid particle dynamics (FPD) method [32,44] for charged colloids [26,27,30] to numerically investigate the nonequilibrium self-assembly of a dilute deionized binary charged colloidal suspension. We demonstrate that, under a constant electric field, oppositely charged colloids form ionic clusters and gels, qualitatively different from bundlelike aggregates formed in free-draining BD

 

simulations. We attribute this difference to the "inverse squeezing flow" effect, which drastically slows down the disaggregation kinetics of colloidal particles induced by the electric field.

Our model consists of $N_p$ cationic colloids of positive charge $Q = Z_p e$ and $N_p$ anionic colloids of negative charge $-Z_p e$ immersed in an implicit solvent characterized by a Bjerrum length $l_B = \beta e^2/(4\pi\varepsilon_{\rm sol})$, where $\beta = 1/(k_B T)$, $k_B$ is Boltzmann's constant, $T$ is the absolute temperature, $\varepsilon_{\rm sol}$ is the dielectric permittivity, and $e$ is the elementary charge. The cationic and anionic colloids have the same diameter $\sigma$ with their charges neutralized by negative (charge $z_{c-}e = -e$) and positive (charge $z_{c+}e = e$) counterions characterized by the continuous number density distribution, $n_{c-}(\boldsymbol{r}, t)$ and $n_{c+}(\boldsymbol{r}, t)$, respectively. The colloidal particles, represented as viscous fluid particles, interact via the Weeks-Chandler-Andersen (WCA) potential with energy coupling $\varepsilon_{\rm WCA}$ and cutoff $r_{\rm cut} = 2^{1/6}\sigma$. The flow field $\boldsymbol{v}$ is calculated by solving the Navier-Stokes (NS) equation [45] and the ion dynamics is described by the Nernst-Planck (NP) equation [46]. To compare with FPD, we conducted BD simulations without thermal noise and HI. Although these simulations should be referred to as Relaxation Dynamics in the strict sense, we call them BD simulations for simplicity. Note that the thermal noise effect is ignored for both FPD and BD. Additional details and parameters are given in Appendix A.

We first investigate the self-assembly of binary charged colloids in the absence of electric fields over a wide range of colloidal charge $Q/e$ (the surface charge density is $\sim 6 \times 10^{-3}$ C/m$^2$ for $Q/e = 500$) and volume fraction $\phi$ (see Fig. 1). For BD simulations without HI [see Fig. 1(a)], we have reproduced the string fluid formation at low $\phi$ whereas the space-spanning percolated network at high $\phi$, in agreement with earlier works [15,18]. Taking the roles of HI into account does not alter the shape of the state diagram qualitatively [see Fig. 1(b)], although the percolation threshold volume fraction increases slightly. Note that, because of the nonequilibrium nature, the threshold volume fraction depends on the observation time, which is $25\tau_{\rm BD}$ here ($\tau_{\rm BD}$ is the Brownian time; see Ref. [47] for the details). While the kinetic pathway is qualitatively the same, the formation of strings and the percolation into a network are significantly retarded under HI [see Fig. 1(b)]. To show this more quantitatively, we characterize the time evolution of the structure by the temporal change of the characteristic wave number $\langle q \rangle$ [see Fig. 1(c)] and find that, for the same colloidal charge $Q/e$, the coarsening dynamics is always slower in FPD than that in BD. The fact that the HI slows down the ordering of colloidal particles is due to the squeezing flow effect [32,34,37,38]; namely, when particles are approaching each other, the solvent between them has to be squeezed out. The squeezing flow effect can be seen by monitoring the temporal change in the distance between two oppositely charged particles. Figure 1(d) clearly shows that the presence of HI slows down the aggregation [32,34,37,38]. From the

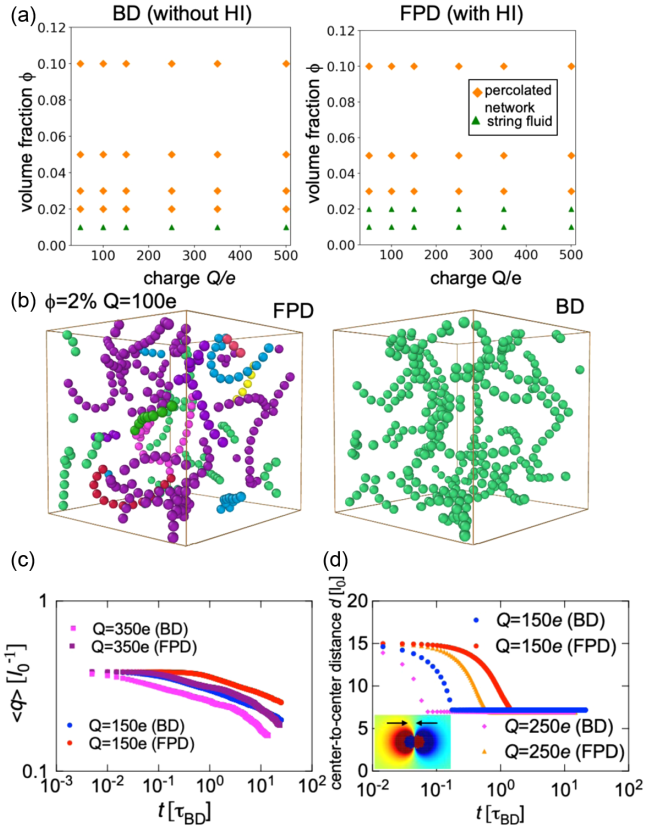


FIG. 1. Self-assembly of binary charged colloidal particles in the absence of electric field. (a) State diagram as a function of colloidal charge $Q/e$ and volume fraction $\phi$ for BD (without HI) and FPD (with HI) simulations at the observation time $t = 25\tau_{\rm BD}$. (b) Simulation snapshots of binary colloids with charge $Q/e = \pm 100$ and volume fraction $\phi = 2\%$ at the time $t = 25\tau_{\rm BD}$. Colors label the connected aggregates with a cutoff $r_c = 10 l_0$. (c) Temporal change of the characteristic wave number $\langle q \rangle$ in BD and FPD simulations of binary colloids of charge $Q/e = \pm 150 - 350$ and volume fraction $\phi = 5\%$. (d) Temporal change of the center-to-center distance between two oppositely charged colloids for BD and FPD. We show the cases for two charge strengths of $Q/e = \pm 150$ and $Q/e = \pm 250$. The presence of HI slows down the aggregation due to the squeezing flow effect [32,34,37,38]. The inset shows the negatively (blue) and positively (red) charged particles approaching each other, with their counterion clouds largely deformed from isotropic shapes.

inset of Fig. 1(d), we see the counterion distribution is largely distorted from the isotropic shape against the basic assumption of screened Yukawa electrostatics.

While the role of HIs only slows down the ordering of charged colloidal particles and does not cause a qualitative change in the above, the situation is remarkably different under an external electric field $E_{\rm ext}$. Figure 2 shows self-assembled structures observed under an electric field with a constant strength $0.2 k_B T/e\ell_0 \simeq 5 \times 10^3$ V cm$^{-1}$ along the $x$ direction. Balancing the electrostatic attractive force $Q^2 l_B k_B T/(e^2\sigma^2)$ between two oppositely charged colloids at close contact with the electric field force $EQ$, we can

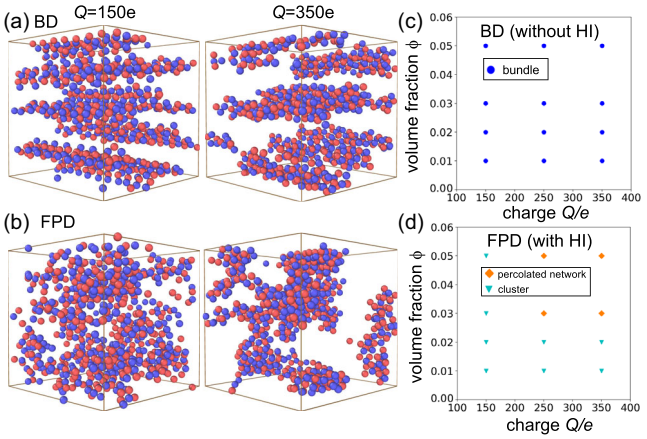


FIG. 2. Self-assembly of binary charged colloidal particles under a constant electric field (see text). (a) Bundlelike aggregates aligned in the field direction observed in BD simulations at $\phi = 5\%$ (see Movies S1 and S2 for left and right panels). (b) Clusters and percolated gels observed in FPD simulations at $\phi = 5\%$ (see Movies S3 and S4 for left and right panels). The full state diagram as a function of colloidal charge $Q/e$ and volume fraction $\phi$ obtained by BD (c) and FPD (d) simulations at the common observation time $t = 25\tau_{\mathrm{BD}}$.

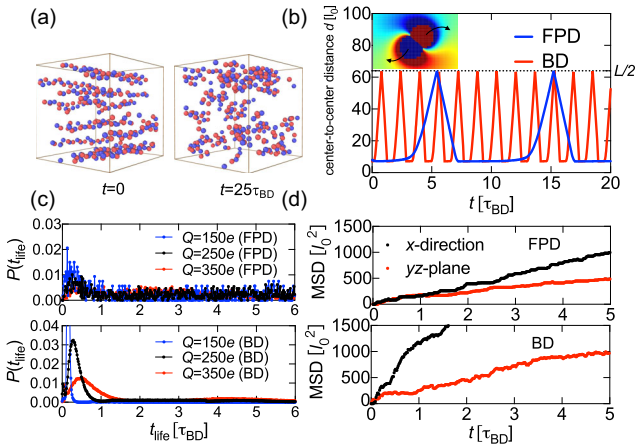


FIG. 3. Origin of the cluster-forming kinetic pathway selected by HI under a constant electric field. (a) With bundlelike aggregates as the initial configuration ($Q/e = \pm 150$ and $\phi = 2\%$), the structure disassembles into colloidal clusters, indicating that the bundlelike aggregates are unstable in FPD. (b) Temporal change of the center-to-center distance between two oppositely charged colloidal particles ($Q/e = \pm 150$) initially closely placed perpendicular to a constant electric field $E_{\mathrm{ext}} = 0.2k_BT/e\ell_0$. HI not only slows down particle aggregation but also decelerates the separation of attached particles. The inset shows the particle pair rotates under the electric field where the counterion cloud is deformed due to the electrostatic interaction with charged colloids and the retardation from ion equilibrium. (c) Probability distribution of binding lifetime $t_{\mathrm{life}}$ suggests enhanced particle binding when the colloidal charge is increased, and HI is considered. The binding lifetime $t_{\mathrm{life}}$ is defined as the time interval between particle attachment ($r \leq 1.5\sigma$) and successive detachment. (d) Mean-square displacement (MSD) in a binary suspension of $Q/e = \pm 350$ and $\phi = 5\%$, showing that the colloidal motions in the $x$ direction and the $yz$ plane are more comparable in FPD than that in BD. The MSD is obtained using reference time $t_0 = 10\tau_{\mathrm{BD}}$.

estimate the critical field strength $E^* = Ql_Bk_BT/(\sigma^2e^2)$, which ranges from 0.2–$0.45k_BT/\ell_0e$ for $Q/e = 150$–350. Thus, the applied electric field of $0.2k_BT/e\ell_0$ is at an intermediate level, not so strong to prevent the structural ordering driven by attraction between oppositely charged colloids. In BD simulations, we observe that colloidal particles self-assemble into bundlelike aggregates consisting of linear strings aligned in the external field direction [Fig. 2(a)] for all the examined cases of colloidal charge $Q/e$ and volume fraction $\phi$ [Fig. 2(c)], qualitatively consistent with earlier BD simulations with the Yukawa potential [17,25]. However, the presence of HIs *even qualitatively* changes the self-assembled structures: colloidal clusters (unlike the linear chains in the field-free case [Fig. 1(b)]) and percolated gels are formed, depending on $Q/e$ and $\phi$ [see Figs. 2(b) and 2(d)]. These results indicate that the HI selects a unique kinetic pathway for binary colloidal self-assembly under a constant external field.

Then, what is the origin of the structural differences? To confirm that the bundlelike aggregates are disfavored in the presence of HI, we conduct an independent FPD simulation under the same condition with the bundlelike aggregates as the initial configuration [Fig. 3(a)]. Indeed, after waiting for $t = 25\tau_{\mathrm{BD}}$, we observe the bundlelike aggregates disassemble into a few colloidal clusters, indicating that the FPD results [Fig. 2(b)] do not depend on the initial configurations. From the radial distribution function (Fig. S1 in [47]), we see in both FPD and BD that the colloidal particles locally arrange into the square lattice structures. Thus, the distinct global structures should result from the selection of the different pathways in the early stage. From the time evolution of colloidal self-assembly (see Supplemental Movies S1–S4), we infer that the stability of bundlelike aggregates in BD comes from the attached oppositely charged colloids being easily separable under an electric field. In other words, a Bjerrum pair made of oppositely charged particles has a short lifetime such that it can be separated before the nearby particles attach to them. This enables oppositely charged particles to roll along the chain, gradually forming bundlelike aggregates aligned in the field direction. On the contrary, the longer lifetime in FPD promotes the gathering of isolated Bjerrum pairs into larger clusters which eventually percolate into the gel network.

To show this, we simulate an elementary model system consisting of two closely spaced colloidal particles with positive and negative charge ($Q = \pm 150e$) under a constant electric field $E_{\mathrm{ext}} = 0.2k_BT/e\ell_0$ and monitor the change in the center-to-center distance $d$ [Fig. 3(b)]. The field is applied perpendicularly to the initial symmetry axis of the two attached particles, leading to the oscillatory change of $d$ in a periodic boundary condition (also see Fig. S2 in [47] for different initial settings). We observe that

HI significantly slows down both the detachment and the reattachment between two colloidal particles, and the former process is slower than the latter because in the former case, the electric field force is partially canceled by the attractive electrostatic force acting in the opposite direction and the particle pair needs to rotate the orientation before separation. This explains the colloid clustering tendency in FPD simulations [Fig. 2(b)]. We also note that the counterion cloud [the inset of Fig. 3(b)] is deformed because of the electrostatic interactions with colloids and the retardation from ion equilibrium, indicating the need to incorporate ion dynamics in particular when an electric field is applied.

The above effects of HI in two-body systems [Fig. 3(b)] also hold in many-particle systems. We can see how HI alters the particle binding under a driving field in Figs. 2(a) and 2(b). There, the presence of HI significantly enhances the lifetime $t_{\mathrm{life}}$ of particle binding compared to the free-draining BD [Fig. 3(c)]; by a factor of 5–8 for the average value $\langle t_{\mathrm{life}} \rangle$ (Fig. S3 in [47]). This indicates that bound particles less readily detach from each other in FPD, helping the formation of cluster aggregates. Analyzing the mean squared displacement (MSD) for a binary suspension of $Q/e = \pm 350$ and $\phi = 5\%$ [see Fig. 3(d)], we find the colloidal mobility along the $x$ direction is slower in FPD and comparable to the motion in the $yz$ plane, which is responsible for the nearly isotropic growth of the cluster, whereas in BD the colloidal motion is predominantly along the $x$ direction, leading to the bundlelike aggregates [Fig. 2(a)].

The slowing down of the separation kinetics of closely spaced particles under HI can be explained by the fact that the solvent must flow into the gap between the particles upon their separation to satisfy the incompressible condition (Fig. S4 in [47]). We call this effect the "inverse squeezing flow" effect since it is the opposite of the solvent squeezing-out effect found in colloidal aggregation [32,34,37,38]. To demonstrate the role of this effect, we study a disaggregation process of a group of 64 oppositely charged colloidal particles initially placed on a cubic lattice to form an ionic crystal configuration [Fig. 5(a)] after the application of a constant electric field of $E_{\mathrm{ext}} = 0.2 k_B T/el_0$. From the temporal change of the degree of asphericity $A$ (see Ref. [47] for the definition) [Fig. 5(b)], we see in BD that the lattice quickly melts to form a bundlelike aggregate [Fig. 5(c)] characterized by $A \approx 1$. On the contrary, the lattice keeps the initial shape for a longer period and slowly evolves into elongated clusters in FPD [Fig. 5(d)]. This demonstrates that the inverse squeezing flow effect decelerates disaggregation between closely spaced particles, responsible for the cluster rather than bundle formation under HI [Fig. 2(b)]. We also show this effect for the explosion of a cluster of like-charge colloids (Fig. S5 in [47]).

Next, we examine the influence of the electric field strength on the structural evolution in gel-forming conditions. We present the structure factor $S(q)$ (see Ref. [47] for the definition) at different times under $E_{\mathrm{ext}} = 0$ and $E_{\mathrm{ext}} = 0.1 k_B T/e\ell_0$ [Fig. 4(a)] and find that in both cases, the height and the position of the $S(q)$ peak grow similarly to spinodal decomposition [20]. We also show the temporal change in the characteristic wave number $\langle q \rangle$ (see Ref. [47] for its definition) under electric fields $E_{\mathrm{ext}} = 0$–$0.4 k_B T/e\ell_0$ in Fig. 4(b). We can see that the growth rate of the characteristic domain size $\langle l \rangle = 2\pi/\langle q \rangle$ nonmonotonically depends on $E_{\mathrm{ext}}$ and becomes maximum at $E^*_{\mathrm{ext}} \approx 0.1$–$0.2 k_B T/e\ell_0$. It indicates that an application of the intermediate electric field accelerates domain coarsening [compare Figs. 4(c) and 4(d)]: Structural reorganization due to field-induced unpairing is difficult for a too weak field. The application of an intermediate electric field can detach pairs of oppositely charged colloids, accelerating the particle dynamics and also increasing the chance of particle contact in various directions (e.g., the number of oppositely charged particles in contact is increased by around 30% at $t = 25\tau_{\mathrm{BD}}$ under $E_{\mathrm{ext}} = 0.2 k_B T/e\ell_0$ compared to the field-free situation). Interestingly, the time evolution of $\langle q \rangle$ follows a power law $\langle q \rangle \sim t^{-1/3}$ for $E_{\mathrm{ext}} = 0.1$–$0.2 k_B T/e\ell_0$ [Fig. 4(b)]. By scaling the wave number $q$ with characteristic $\langle q \rangle$, we find the structure factors are collapsed on a single master curve as $\langle q \rangle^3 S(q,t) = g(q/\langle q \rangle)$ where $g(\cdots)$ denotes some function (Fig. S6 in [47]). Chord length distributions for the pore size of the network $P(\ell_{\mathrm{out}})$ at various times also collapse onto a single master curve after scaling the pore size $\ell_{\mathrm{out}}$ (see Ref. [47] for the definition) by $\langle \ell \rangle$ (Fig. S6 in [47]). These

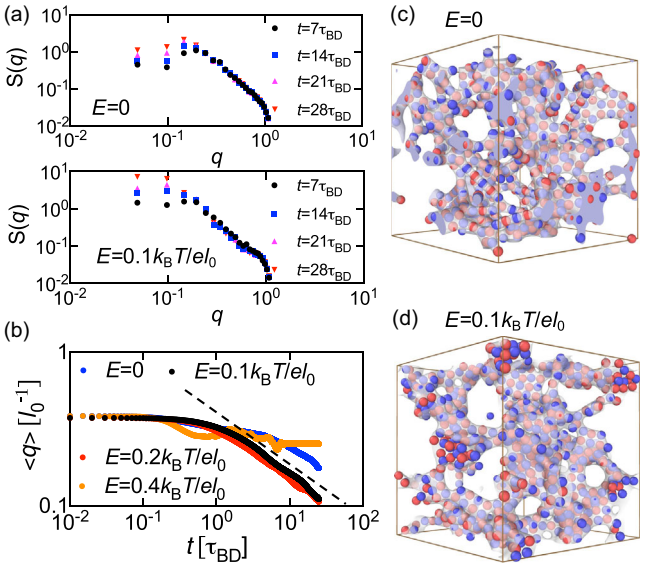


FIG. 4. Effects of the electric field strength on the gel formation in a binary suspension of charge $Q/e = \pm 250$ and volume fraction $\phi = 5\%$ with HI. (a) Structure factor $S(q,t)$ at different times $t = 7$–$28\tau_{\mathrm{BD}}$ for gels under $E_{\mathrm{ext}} = 0$ and $E_{\mathrm{ext}} = 0.1 k_B T/e\ell_0$. (b) Temporal change of the characteristic wave number $\langle q \rangle$ under various field strengths ranging from 0 to $0.4 k_B T/e\ell_0$. The dashed line has a slope of $-1/3$. (c) and (d) The snapshots of binary gels formed under $E_{\mathrm{ext}} = 0$ and $E_{\mathrm{ext}} = 0.1 k_B T/e\ell_0$ at the observation time $t = 25\tau_{\mathrm{BD}}$. Here, we use the Gaussian blurring to show the network topology.

results confirm the self-similar nature of isotropic network coarsening, although there is slight anisotropicity in $S(\boldsymbol{q})$ for $E_{\rm ext} = 0.2k_BT/e\ell_0$ (Fig. S7 in [47]). However, we need further careful studies of the underlying mechanism behind the network coarsening law under an external field.

Finally, we discuss the validity and deficiency of the adiabatic approximation for counterion clouds, often employed in simulations (Figs. S8–S12 in [47]). Although the self-assembly structures look similar between simulations with ion dynamics and adiabatic approximation, there are noticeable differences in particle-level structural development (Figs. S8–S11 in [47]) and counterion distribution (Fig. S12 in [47]). Thus, we need special care for applying the adiabatic approximation for many-body problems.

In conclusion, using the fluid particle dynamics method [32,44] for charged colloids [26,27,30], we have elucidated the crucial roles of hydrodynamic interactions and electric fields in the nonequilibrium self-assembly of a dilute binary suspension of oppositely charged colloids. We have shown that without an external field, HI slows down the ordering of colloidal particles due to the squeezing flow effect, although the structures formed are qualitatively similar to the BD simulation case. However, the situation is remarkably different when we apply a constant electric field: binary oppositely charged colloidal particles form ionic clusters and percolate into gels with enhanced domain thickness compared to the field-free situation. The structures fundamentally differ from those in BD simulations, where bundlelike aggregates of linear chains are formed. We have revealed that the clustering of colloidal particles under the external field originates from the "inverse squeezing flow" effect that dramatically slows down the disaggregation of colloidal clusters due to the incompressibility of the fluid component. These findings emphasize the need to consider hydrodynamics, especially short-range many-body parts, for predicting nonequilibrium colloidal self-assembly, particularly for low salt concentration and colloidal volume fraction (we briefly discuss the relationship of our findings to existing experiments in Appendix C). Our Letter provides fresh insights into the roles of hydrodynamics and electric fields in charged colloid assembly and hints at experimentally controlling binary gels' structures.

This work was supported by the Grant-in-Aid for Specially Promoted Research (JSPS KAKENHI Grant No. JP20H05619) from the Japan Society for the Promotion of Science (JSPS).

*Appendix A: Simulation details.*—We explain the FPD method for charged colloidal suspensions [26,27,30,32,44]. In the FPD method, colloidal particles are represented as viscous fluid particles expressed as

$$\psi_i(\boldsymbol{r}) = \frac{1}{2}\{\tanh[(a - |\boldsymbol{r} - \boldsymbol{R}_i|)/\xi] + 1\}, \tag{A1}$$

where $a$ is the particle radius, $\xi$ is the interface thickness, and $\boldsymbol{R}_i$ is the position vector of the center of mass of the particle with index $i$. In this way, we obtain a smooth phase field $\psi(\boldsymbol{r}) = \sum_{i=1}^{2N_p} \psi_i(\boldsymbol{r})$ and viscosity field

$$\eta(\boldsymbol{r}) = \eta_s + (\eta_p - \eta_s)\psi(\boldsymbol{r}), \tag{A2}$$

with $\eta_s$ and $\eta_p$ the viscosities of fluid and particles. By choosing $\eta_{\rm p} = 50\eta_s$, the flow gradient inside the particle becomes negligible, and each particle can be safely regarded as a rigid particle [32,44]. The surface charge density of colloidal particle $i$ is given as $\rho_{\rm pi}(\boldsymbol{r}, t) = Z_i e|\nabla\psi_i(\boldsymbol{r}, t)|/A_i$, where $Z_i = \pm Z_p$ and $A_i = \int d\boldsymbol{r}|\nabla\psi_i(\boldsymbol{r}, t)|$ is the surface area in the limit of $\xi/a \to 0$. The flow field $\boldsymbol{v}$ is calculated by solving the Navier-Stokes (NS) equation

$$\rho\left(\frac{\partial}{\partial t} + \boldsymbol{v}\cdot\nabla\right)\boldsymbol{v} = \boldsymbol{f} + \nabla\cdot\overleftrightarrow{\boldsymbol{\sigma}} - \sum_\alpha n_\alpha\nabla\mu_\alpha, \tag{A3}$$

where $\rho$ is the constant fluid density, $\boldsymbol{f} = \sum_i \boldsymbol{F}_i\psi_i(\boldsymbol{r})/\int\psi_i(\boldsymbol{r}')d\boldsymbol{r}'$ is the force field by smearing out the interaction force $\boldsymbol{F}_i$ of colloids, $n_\alpha$ is the number distribution of counterion, $\overleftrightarrow{\boldsymbol{\sigma}} = \eta(\boldsymbol{r})[\nabla\boldsymbol{v} + (\nabla\boldsymbol{v})^T] - p\overleftrightarrow{\boldsymbol{I}}$ is the internal stress of the fluid, $p$ is the pressure determined to satisfy the incompressible condition $\nabla\cdot\boldsymbol{v} = 0$, and $\overleftrightarrow{\boldsymbol{I}}$ is the unit tensor. The term $\mu_\alpha$ is the chemical potential of counterions ($\alpha = c+, c-$) given as $\beta\mu_\alpha = \beta e z_\alpha\Phi + \ln(n_\alpha v_0) + g_c\psi$, where $\Phi$ is the electrostatic potential, $z_\alpha = \pm 1$, $v_0$ is the ion's volume, and the constant $g_c$ is introduced to avoid ion permeation into colloidal particles. The interaction force $\boldsymbol{F}_i$ acting on colloid $i$ reads $\boldsymbol{F}_i = -\partial U_{\rm WCA}/\partial\boldsymbol{R}_i + \int d\boldsymbol{r}(\sum_\alpha k_BTg_cn_\alpha\nabla\psi_i - \rho_{\rm pi}\nabla\Phi)$, which contains the contribution from the Weeks-Chandler-Andersen (WCA) interaction $U_{\rm WCA}$, the counterion exclusion term, and the electrostatic forces. The position of colloidal particle $i$ is updated as a rigid body by $d\boldsymbol{R}_i/dt = \boldsymbol{V}_i$, where $\boldsymbol{V}_i = \int d\boldsymbol{r}\boldsymbol{v}\psi_i/\int d\boldsymbol{r}\psi_i$ is the particle velocity. We solve the NS equation by the marker-and-cell (MAC) method with a staggered lattice under periodic boundary condition [45]. The ion dynamics is described by the Nernst-Planck (NP) equation

$$\frac{\partial}{\partial t}n_\alpha = -\boldsymbol{v}\cdot\nabla n_\alpha + \nabla\cdot D_\alpha n_\alpha\nabla(\beta\mu_\alpha), \tag{A4}$$

where $D_\alpha$ is the ion diffusion constant. The electrostatic potential $\Phi$ is updated by solving the Poisson equation $-\varepsilon_{\rm sol}\nabla^2\Phi = \rho_{\rm e}$, where the spatial homogeneity of $\varepsilon_{\rm sol}$ is assumed, $\rho_{\rm e}$ is the total charge density given as $\rho_{\rm e} = \rho_{\rm p} + \sum_{\alpha=(c+,c-)} z_\alpha e n_\alpha$, and $\rho_{\rm p}(\boldsymbol{r}, t) = \sum_i \rho_{\rm pi}(\boldsymbol{r}, t)$ is the colloidal charge density. For simplicity, we neglect

thermal fluctuation terms in the NS and NP equations, which is a reasonable approximation because the energy scales of electrostatic interactions and particle-electric field interactions far exceed $k_BT$. The initial homogenous configurations were prepared by the equilibrium simulations of colloidal particles, which interact through the WCA interaction. The system is three-dimensional periodic with a length $L = 128l_0$ in each direction, where $l_0$ is the lattice size.

For modeling the solvent, we use mass density $\rho = 1\ g/\mathrm{cm}^3$, solvent viscosity $\eta_s = 10^{-3}$ Pa s and $l_B = 0.7$ nm, corresponding to water at room temperature of $T = 300$ K. For modeling the colloids, we use $a = 3.2l_0$, $\xi = l_0$, $\sigma = 2a + \xi = 7.4l_0$, $g_c = 15$, and $\varepsilon_{\mathrm{WCA}} = 10k_BT$. The volume of an ion, $v_0$, is set to be $v_0 = (0.3\ \mathrm{nm})^3$. We set the length unit as $l_0 = 10$ nm, the energy unit as $k_BT$, the velocity unit as $v = k_BT/(\eta_s l_0^2)$, and the time unit as $t_0 = \eta_s l_0^3/(k_BT) \simeq 2.42 \times 10^{-7}$ s. With these parameters, the Reynolds number of the fluid is $\mathrm{Re} = \rho v \ell_0/\eta_s \simeq 4.14 \times 10^{-4} \ll 1$, indicating the fluid exhibits Stokes flow behavior. In the NP equation, we set $D_\alpha = 2.4\ell_0^2/t_0 \simeq 10^{-5}\ \mathrm{cm}^2\ \mathrm{s}^{-1}$ which is a typical diffusion constant of ions. The simulation time step is $\Delta t = 2.5 \times 10^{-3} t_0$ which is scaled by the Brownian time of an isolated colloid $\tau_{\mathrm{BD}} = a_H^2/6D_c$, where $a_H = 1.04a$ is the hydrodynamic radius [44], $D_c = k_BT/(6\pi a_H \eta_s \lambda) = 9.4 \times 10^{-3}\ell_0^2/t_0 \simeq 3.9 \times 10^{-8}\ \mathrm{cm}^2/s$ is the colloidal diffusion constant, and $\lambda = \int \psi(\boldsymbol{r})d\boldsymbol{r}/\int \psi(\boldsymbol{r})^2 d\boldsymbol{r}$ is a correction factor in FPD, yielding $\Delta t \simeq 1.28 \times 10^{-5}\tau_{\mathrm{BD}}$.

To make comparisons with FPD, we also conducted Brownian dynamics (BD) simulations by calculating the time evolution of particle position and ion dynamics as $\zeta \boldsymbol{V}_i = \boldsymbol{F}_i$ and $(\partial/\partial t)n_\alpha = \nabla \cdot D_\alpha n_\alpha \nabla(\beta\mu_\alpha)$, where $\zeta = k_BT/D_c \simeq 1.06 \times 10^2 \eta_s l_0$ is the damping coefficient.

Instead of modeling ion dynamics with the NP equation, the adiabatic approximation of the counterion cloud (corresponding to constant chemical potential $\beta\mu_\alpha$) is often employed in colloid simulations such that the electrostatic potential $\Phi$ can be obtained by solving the Poisson-Boltzmann (PB) equation $-\varepsilon_{\mathrm{sol}}\nabla^2\Phi = \rho_e$, where $\rho_e$ is the total charge density given as $\rho_e = \rho_p + \sum_\alpha Z_p N_p z_\alpha e C_\alpha^{-1} e^{-\beta(z_\alpha e\Phi + g\psi)}$, $\rho_p(\boldsymbol{r}, t) = \sum_i \rho_{pi}(\boldsymbol{r}, t)$ represents the colloidal charge density, and $C_\alpha = \int d\boldsymbol{r} e^{-\beta(z_\alpha e\Phi + g\psi)}$ is a normalization factor. We discuss the validity and deficiency of the adiabatic approximation in [47].

*Appendix B: Demonstration of the inverse squeezing flow.*—Figure 5 shows a disaggregation process of a group of 64 oppositely charged colloidal particles initially placed on a cubic lattice under external electric field $E_{\mathrm{ext}} = 0.2k_BT/el_0$, which is a demonstration of the inverse squeezing flow effect in many-body systems.

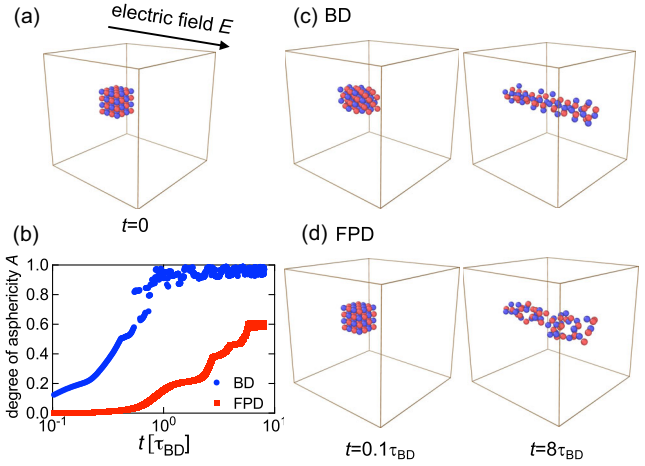


FIG. 5. Demonstration of the impact of the inverse squeezing flow effect. (a) A disaggregation process of 64 oppositely charged ($Q/e = \pm 150$) particles initially placed on the cubic lattice with lattice constant $8l_0$ after applying a constant electric field with strength $E_{\mathrm{ext}} = 0.2k_BT/el_0$. (b) The temporal change of the degree of asphericity $A$. (c) Formation of a bundlelike aggregate in BD simulation. (d) Irregular-shaped elongated cluster formation in FPD simulation.

*Appendix C: Connection between computational model and experiments.*—We discuss the connection of our model system to the existing experiments of binary oppositely charged colloidal mixtures. In our model, the diameter of colloidal particles is $\sigma = 74$ nm and the Bjerrum length $l_B = 0.7$ nm. The Debye screening length is around $l_{\mathrm{Debye}} = 45 \sim 29$ nm for $Q/e = 150 \sim 350$ in our system, where only the counterions are taken into account since the system is salt-free. Hitherto, emphasis has primarily been on the lane formation and jammed bonds formed in binary oppositely charged colloidal mixtures in the pioneering experiments [10,23]. In these experiments [10,23], the diameter of colloidal particles is around 1–2 μm and the typical screening length is 200–300 nm. Thus, the Debye screening length scaled by the particle size is much larger in our model than the experiments, especially for a lower colloidal charge. Moreover, the volume fraction $\phi$ of colloidal particles in these experiments [10,23] is typically above 15%, which is higher than the one we considered here ($\phi < 10\%$) since the correlations between the particles are not sufficient to form lanes or bands in the regime of a low volume fraction. These differences may explain why previous free-draining BD simulations [19,20,22,23,25] with Yukawa electrostatics often qualitatively explain the experimental structures [10,23] since both electrostatics and HI can be effectively screened.

We expect that our findings provide insight into the nonequilibrium colloidal self-assembly under longer-ranged electrostatics and HI, which to our knowledge, has not been examined in experiments. Therefore, we hope our results will encourage researchers to verify our

computational prediction in experiments, enhancing our fundamental understanding of the critical roles of hydrodynamic interactions in soft matter and biological systems.

*yuan@g.ecc.u-tokyo.ac.jp
†takae@iis.u-tokyo.ac.jp
‡tanaka@iis.u-tokyo.ac.jp

[1] Zhenli Zhang and Sharon C. Glotzer, Self-assembly of patchy particles, Nano Lett. **4**, 1407 (2004).
[2] Liang Hong, Angelo Cacciuto, Erik Luijten, and Steve Granick, Clusters of charged Janus spheres, Nano Lett. **6**, 2510 (2006).
[3] Pinar Akcora, Hongjun Liu, Sanat K. Kumar, Joseph Moll, Yu Li, Brian C. Benicewicz, Linda S. Schadler, Devrim Acehan, Athanassios Z. Panagiotopoulos, Victor Pryamitsyn, Venkat Ganesan, Jan Ilavsky, Pappanan Thiyagarajan, Ralph H. Colby, and Jack F. Douglas, Anisotropic self-assembly of spherical polymer-grafted nanoparticles, Nat. Mater. **8**, 354 (2009).
[4] Qian Chen, Erich Diesel, Jonathan K. Whitmer, Sung Chul Bae, Erik Luijten, and Steve Granick, Triblock colloids for directed self-assembly, J. Am. Chem. Soc. **133**, 7725 (2011).
[5] Qian Chen, Sung Chul Bae, and Steve Granick, Directed self-assembly of a colloidal kagome lattice, Nature (London) **469**, 381 (2011).
[6] Matthew R. Jones, Robert J. Macfarlane, Andrew E. Prigodich, Pinal C. Patel, and Chad A. Mirkin, Nanoparticle shape anisotropy dictates the collective behavior of surface-bound ligands, J. Am. Chem. Soc. **133**, 18865 (2011).
[7] Alexander M. Kalsin, Marcin Fialkowski, Maciej Paszewski, Stoyan K. Smoukov, Kyle J. M. Bishop, and Bartosz A. Grzybowski, Electrostatic self-assembly of binary nanoparticle crystals with a diamond-like lattice, Science **312**, 420 (2006).
[8] David A. Walker, Kevin P. Browne, Bartlomiej Kowalczyk, and Bartosz A. Grzybowski, Self-assembly of nanotriangle superlattices facilitated by repulsive electrostatic interactions, Angew. Chem., Int. Ed. **49**, 6760 (2010).
[9] Marjolein Dijkstra and Erik Luijten, From predictive modelling to machine learning and reverse engineering of colloidal self-assembly, Nat. Mater. **20**, 762 (2021).
[10] Mirjam E. Leunissen, Christina G. Christova, Antti-Pekka Hynninen, C. Patrick Royall, Andrew I. Campbell, Arnout Imhof, Marjolein Dijkstra, Rene Van Roij, and Alfons Van Blaaderen, Ionic colloidal crystals of oppositely charged particles, Nature (London) **437**, 235 (2005).
[11] Elena V. Shevchenko, Dmitri V. Talapin, Nicholas A. Kotov, Stephen O'Brien, and Christopher B. Murray, Structural diversity in binary nanoparticle superlattices, Nature (London) **439**, 55 (2006).
[12] A. P. Hynninen, C. G. Christova, R. van Roij, A. van Blaaderen, and M. Dijkstra, Prediction and Observation of Crystal Structures of Oppositely Charged Colloids, Phys. Rev. Lett. **96**, 138308 (2006).
[13] Eduardo Sanz, Chantal Valeriani, Teun Vissers, Andrea Fortini, Mirjam E. Leunissen, Alfons van Blaaderen, Daan Frenkel, and Marjolein Dijkstra, Out-of-equilibrium processes in suspensions of oppositely charged colloids: Liquid-to-crystal nucleation and gel formation, J. Phys. Condens. Matter **20**, 494247 (2008).
[14] Manuel S. Romero-Cano, José B. Caballero, and Antonio M. Puertas, Experimental phase diagram of symmetric binary colloidal mixtures with opposite charges, J. Phys. Chem. B **110**, 13220 (2006).
[15] Rui Zhang, Prateek K. Jha, and Monica Olvera de la Cruz, Non-equilibrium ionic assemblies of oppositely charged nanoparticles, Soft Matter **9**, 5042 (2013).
[16] Bhuvnesh Bharti, Gerhard H. Findenegg, and Orlin D. Velev, Co-assembly of oppositely charged particles into linear clusters and chains of controllable length, Sci. Rep. **2**, 1004 (2012).
[17] Frank Smallenburg, Hanumantha Rao Vutukuri, Arnout Imhof, Alfons Van Blaaderen, and Marjolein Dijkstra, Self-assembly of colloidal particles into strings in a homogeneous external electric or magnetic field, J. Phys. Condens. Matter **24**, 464113 (2012).
[18] Ahmet Faik Demirörs, Johan C. P. Stiefelhagen, Teun Vissers, Frank Smallenburg, Marjolein Dijkstra, Arnout Imhof, and Alfons van Blaaderen, Long-Ranged Oppositely Charged Interactions for Designing New Types of Colloidal Clusters, Phys. Rev. X **5**, 021012 (2015).
[19] Kulveer Singh, Anubhav Raghav, Prateek K. Jha, and Soumitra Satapathi, Effect of size and charge asymmetry on aggregation kinetics of oppositely charged nanoparticles, Sci. Rep. **9**, 3762 (2019).
[20] Eduardo Sanz, Mirjam E. Leunissen, Andrea Fortini, Alfons van Blaaderen, and Marjolein Dijkstra, Gel formation in suspensions of oppositely charged colloids: Mechanism and relation to the equilibrium phase diagram, J. Phys. Chem. B **112**, 10861 (2008).
[21] M. A. Piechowiak, A. Videcoq, R. Ferrando, D. Bochicchio, C. Pagnoux, and F. Rossignol, Aggregation kinetics and gel formation in modestly concentrated suspensions of oppositely charged model ceramic colloids: A numerical study, Phys. Chem. Chem. Phys. **14**, 1431 (2012).
[22] Emily R. Russell, Joris Sprakel, Thomas E. Kodger, and David A. Weitz, Colloidal gelation of oppositely charged particles, Soft Matter **8**, 8697 (2012).
[23] Teun Vissers, Adam Wysocki, Martin Rex, Hartmut Löwen, C Patrick Royall, Arnout Imhof, and Alfons van Blaaderen, Lane formation in driven mixtures of oppositely charged colloids, Soft Matter **7**, 2352 (2011).
[24] Shin-Hyun Kim, Su Yeon Lee, Seung-Man Yang, and Gi-Ra Yi, Self-assembled colloidal structures for photonics, Nat. Mater. **3**, 25 (2011).
[25] M. Rex and H. Löwen, Lane formation in oppositely charged colloids driven by an electric field: Chaining and two-dimensional crystallization, Phys. Rev. E **75**, 051402 (2007).
[26] Hiroya Kodama, Kimiya Takeshita, Takeaki Araki, and Hajime Tanaka, Fluid particle dynamics simulation of charged colloidal suspensions, J. Phys. Condens. Matter **16**, L115 (2004).
[27] Takeaki Araki and Hajime Tanaka, Physical principle for optimizing electrophoretic separation of charged particles, Europhys. Lett. **82**, 18004 (2008).

[28] Kang Kim, Yasuya Nakayama, and Ryoichi Yamamoto, Direct Numerical Simulations of Electrophoresis of Charged Colloids, Phys. Rev. Lett. **96**, 208302 (2006).
[29] Roman Schmitz and Burkhard Dünweg, Numerical electrokinetics, J. Phys. Condens. Matter **24**, 464111 (2012).
[30] Kyohei Takae and Hajime Tanaka, Hydrodynamic simulations of charge-regulation effects in colloidal suspensions, Soft Matter **14**, 4711 (2018).
[31] Akira Onuki, *Phase Transition Dynamics* (Cambridge University Press, Cambridge, England, 2002).
[32] Hajime Tanaka and Takeaki Araki, Simulation Method of Colloidal Suspensions with Hydrodynamic Interactions: Fluid Particle Dynamics, Phys. Rev. Lett. **85**, 1338 (2000).
[33] Hajime Tanaka and Takeaki Araki, Spontaneous coarsening of a colloidal network driven by self-generated mechanical stress, Europhys. Lett. **79**, 58003 (2007).
[34] Akira Furukawa and Hajime Tanaka, Key Role of Hydrodynamic Interactions in Colloidal Gelation, Phys. Rev. Lett. **104**, 245702 (2010).
[35] Michio Tateno and Hajime Tanaka, Numerical prediction of colloidal phase separation by direct computation of Navier–Stokes equation, npj Comput. Mater. **5**, 40 (2019).
[36] Michio Tateno and Hajime Tanaka, Power-law coarsening in network-forming phase separation governed by mechanical relaxation, Nat. Commun. **12**, 912 (2021).
[37] Kumiko Kamata, Takeaki Araki, and Hajime Tanaka, Hydrodynamic Selection of the Kinetic Pathway of a Polymer Coil-Globule Transition, Phys. Rev. Lett. **102**, 108303 (2009).
[38] Hajime Tanaka, Roles of hydrodynamic interactions in structure formation of soft matter: Protein folding as an example, J. Phys. Condens. Matter **17**, S2795 (2005).
[39] Fabio C. Zegarra, Dirar Homouz, Yossi Eliaz, Andrei G. Gasic, and Margaret S. Cheung, Impact of hydrodynamic interactions on protein folding rates depends on temperature, Phys. Rev. E **97**, 032402 (2018).
[40] Martin Rex and Hartmut Löwen, Influence of hydrodynamic interactions on lane formation in oppositely charged driven colloids, Eur. Phys. J. E **26**, 143 (2008).
[41] Hiroshi Yoshida, Norio Ise, and Takeji Hashimoto, Void structure and vapor–liquid condensation in dilute deionized colloidal dispersions, J. Chem. Phys. **103**, 10146 (1995).
[42] N. Lutterbach, H. Versmold, V. Reus, L. Belloni, and Th. Zemb, Charge-stabilized liquidlike ordered binary colloidal suspensions. 1. Ultra-small-angle X-ray scattering characterization, Langmuir **15**, 337 (1999).
[43] Nina J. Lorenz, Hans Joachim Schöpe, Holger Reiber, Thomas Palberg, Patrick Wette, Ina Klassen, Dirk Holland-Moritz, Dieter Herlach, and Tsuneo Okubo, Phase behaviour of deionized binary mixtures of charged colloidal spheres, J. Phys. Condens. Matter **21**, 464116 (2009).
[44] Akira Furukawa, Michio Tateno, and Hajime Tanaka, Physical foundation of the fluid particle dynamics method for colloid dynamics simulation, Soft Matter **14**, 3738 (2018).
[45] Francis H. Harlow and J. Eddie Welch, Numerical calculation of time dependent viscous incompressible flow of fluid with free surface, Phys. Fluids **8**, 2182 (1965).
[46] Ronald F. Probstein, *Physicochemical Hydrodynamics: An Introduction* (John Wiley & Sons, New York, 2005).
[47] See Supplemental Material at http://link.aps.org/supplemental/10.1103/PhysRevLett.129.248001 for information about the analysis methods, the additional characterization (the radial distribution function, reattachment and detachment between two particles under field, binding lifetime of particle pair, additional demonstration of inverse squeezing flow, structure factors and pore size distribution, and validity and deficiency of the adiabatic approximation for counterion clouds), and the movies of phase ordering kinetics under an electric field.